Appendix A. Supplementary data

Enhancing CO_2 Photoreduction through Unique 2D MOF-Based Heterostructures with Metalloid Doping

Xiaoxiong Hou[a], Zhuangzhuang Ma[a], Zhilei Zhang[b,c], Peijin Zou[a],, Hongqiang Wang[d*], Lichao Jia[a*]

[a] *Key Laboratory of Applied Surface and Colloid Chemistry, National Ministry of Education, Shaanxi Key Laboratory for Advanced Energy Devices, Shaanxi Engineering Lab for Advanced Energy Technology, School of Materials Science and Engineering, Shaanxi Normal University, 620 West Chang'an Street, Xi'an, Shaanxi 710119, China*

[b] *Beijing National Laboratory for Molecular Sciences, Key Laboratory of Organic Solids, Institute of Chemistry, Chinese Academy of Sciences, Beijing 100190, China.*

[c] *University of the Chinese Academy of Sciences, Beijing 100049, China.*

[d] *State Key Laboratory of Solidification Processing, Center for Nano Energy Materials, School of Materials Science and Engineering, Northwestern Polytechnical University and Shaanxi Joint Labortary of Graphene, Xi'an, 710072, P. R. China*

* Corresponding author.

E-mail: hongqiang.wang@nwpu.edu.cn; lichaojia@snnu.edu.cn

1. Sample preparation

0.33 g $Zn(NO_3)_2 \cdot 6H_2O$ and 0.985 g 2-methylimidazole were dissolved in 90 mL H_2O, respectively, and stirred for 30 min to form a clear solution A and B. The obtained solution A was added into the solution B, the mixture solution was kept stirring for 24 h at room temperature. The obtained product was filtered and washed with water and ethanol for three times, and dried in an vacuum oven under 65 ℃ named ZIF-8 nanosheet (ZIF-8NS).

2. The test of photoelectrochemical and efficiency

The mott-Schottky test can be used to determine the type of semiconductor and the flat band potential of the semiconductor material. Combined with the band gap of the semiconductor measured by UV-VIS analysis, the position of the valence band of the semiconductor material can be estimated. The adopted three-electrode working system was tested under dark condition with a voltage range of -0.5-0.7 VAg/AgCl and a working frequency of 1000 Hz. The carrier concentration of the semiconductor was calculated by formula 1.1 and 1.2 combined with the slope of the curve.

$$\frac{1}{C^2} = 2(V_s - V_f - \frac{kT}{e})/(e\varepsilon_0 \varepsilon N_d A^2) \tag{1.1}$$

$$N_d = \left(\frac{2}{e\varepsilon_0 \varepsilon}\right) \times \left(\frac{d\left(\frac{1}{C2}\right)}{dVs}\right)^{-1} \tag{1.2}$$

C, ***e***, V_s, V_f, ***K***, N_d, ***A***, ε_0, ε and $d(1/C^2)/dV_s$ are representation of space charge capacitance, charge amount of an electron, external bias, flat band potential, Boltzmann constant, donor concentration of N-type semiconductor, test area of photoanode, vacuum dielectric constant 8.854×10^{-12} Fm^{-1}, relative dielectric constant of CuO (10.26)

and ZIF-8 (1.82) and the slope of Motschottky curve, respectively.

The carrier transfer efficiency of catalysts can be measured by Electrochemistry Impedance Spectroscope (EIS). The test conditions are as follows: the test frequency range is 0.1-1 MHZ under dark state condition. The bias of the perturbation signal is 10 mV. Current density-Voltage (J-V) curve can be measured at voltage range of -0.6-1.2 $V_{Ag/AgCl}$, and the voltage scan speed is 10 mvs^{-1} in the light condition. The potential of the photoelectric pole is converted to a relative reversible hydrogen electrode by the Nernst:

$$V_{RHE} = V_{Ag/Cl} + 0.197 + 0.0591V \times pH \quad (1.3)$$

$$V_{NHE} = V_{Ag/Cl} + 0.197 \quad (1.4)$$

Before measurement of transient current spectrum (I-T), the light intensity of the light source was adjusted to 100 $mW \cdot cm^{-2}$, and time and bias are set to 500 seconds and 10 mV, respectively. The sample was illuminated with the light source for 30 seconds before the light source was blocked first, and then the light was shaded for 30 seconds. Repeat this procedure until the end of time. Working electrode was put into the system to stabilize before start collecting data to record its current change. The current magnitude was detected under open circuit voltage.

Calculation of Apparent Quantum Yield (QE%):

The apparent quantum yield (QE) is defined as the ratio of number of reacted electrons to the number of incident photons. In general, two electrons are required to produce one CO molecule, whereas, eight electrons are needed to produce one CH_4 molecule. The apparent quantum yield (QE) measurement was performed using the

equation below:

$$QE(\%) = \frac{2 \times N_a \times N_{(CO)} + 8 \times N_a \times N_{(CH_4)}}{I \times A \times \frac{\lambda}{hc} \times t} \times 100\% \quad (1.5)$$

where, $N_{(CO)}$ is number of CO (mole) evolved and $N_{(CH4)}$ is number of CH_4 (mole) evolved in time "t" (1 h), Na is Avogadro's number (N = 6.022 × $10^{23}$$mol^{-1}$), I is the incident solar irradiance (I=1.89 mW cm^{-2}), 300 W Xenon lamp (Beijing Zhongjiaojinyuan Technology Co. Ltd., China) was positioned 10 cm above the reactor, and the focused areas in the reactor for the lamp was 28.26 cm^2. λ is the wavelength of the study (379 nm), h is Planck's constant (6.62×10^{-34} J·s), c is the speed of light (3.0×108 m s^{-1}).

Energy Conversion Efficiency (CE%):

$$CE(\%) = \frac{\Delta H_{(CO)} \times N_{(CO)} + \Delta H_{(CH_4)} \times N_{(CH_4)}}{I \times A \times t} \times 100\% \quad (1.6)$$

where, $N_{(CO)}$ is number of CO (183.33 μmol, mole) evolved and $N_{(CH4)}$ is number of CH_4 (32.67 μmol, mole) evolved in time "t" (1 h), $\Delta H_{(CO)}$ is heat of combustion of CO ($\Delta H_{(CO)}$= 283.0 kJ mol^{-1}) and $\Delta H_{(CH_4)}$ is heat of combustion of CH_4 ($\Delta H_{(CH_4)}$ = 890.0 kJ mol^{-1}), I is the incident solar irradiance (I = 500 mW cm^{-2}) over the exposed irradiated area A (28.26 cm^2).

Mechanism of CO_2 reduction:

$$CO_2 + 2H^+ + 2e^- \rightarrow CO\uparrow + H_2O \quad E = -0.52\,V \quad (E1)$$

$$CO_2 + 2H^+ + 2e^- \rightarrow HCOOH \quad E = -0.61\,V \quad (E2)$$

$$CO_2 + 4H^+ + 4e^- \rightarrow HCHO + H_2O \quad E = -0.48\,V \quad (E3)$$

$$CO_2 + 6H^+ + 6e^- \rightarrow CH_3OH + H_2O \quad E = -0.32\,V \quad (E4)$$

$$CO_2 + 8H^+ + 8e^- \rightarrow CH_4\uparrow + 2H_2O \quad E = -0.24\,V \quad (E5)$$

$$4OH^+ - 4e^- \rightarrow O_2\uparrow + 2H_2O \quad E = 0.82\,V \quad (E6)$$

1. Figures

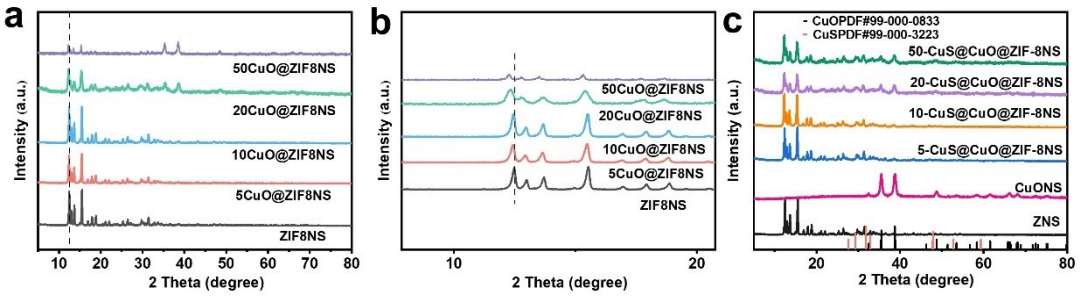

Figure S1. XRD (a), HRXRD (b) patterns of CuO@ZIF-8NS and (c) XRD of CuS@CuO@ZIF-8NS.

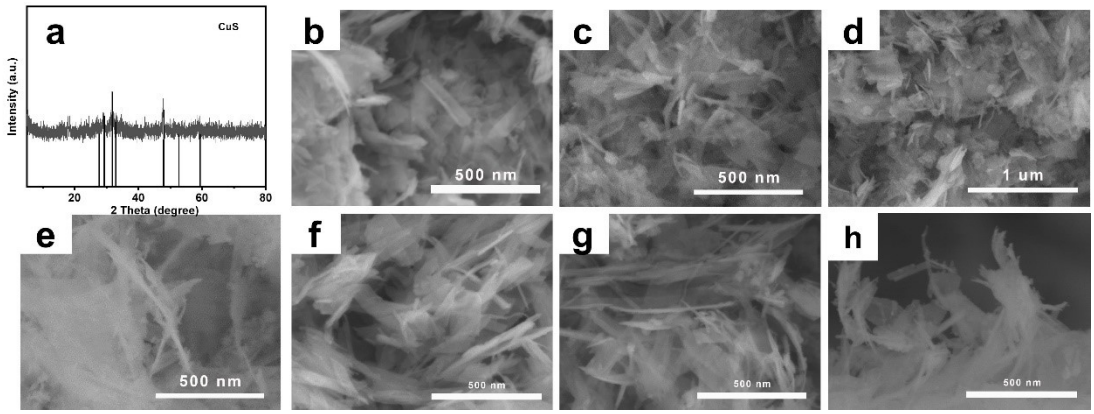

Figure S2. XRD patterns of naked CuS (a); SEM images of samples with different time and temperature: (b) 5 min-80 ℃, (c) 10 min-80 ℃, (d) 20 min-80 ℃, (e) 40 min-80 ℃, (f) 10 min-30 ℃, (g) 10 min-60 ℃ and (h) 10 min-100 ℃.

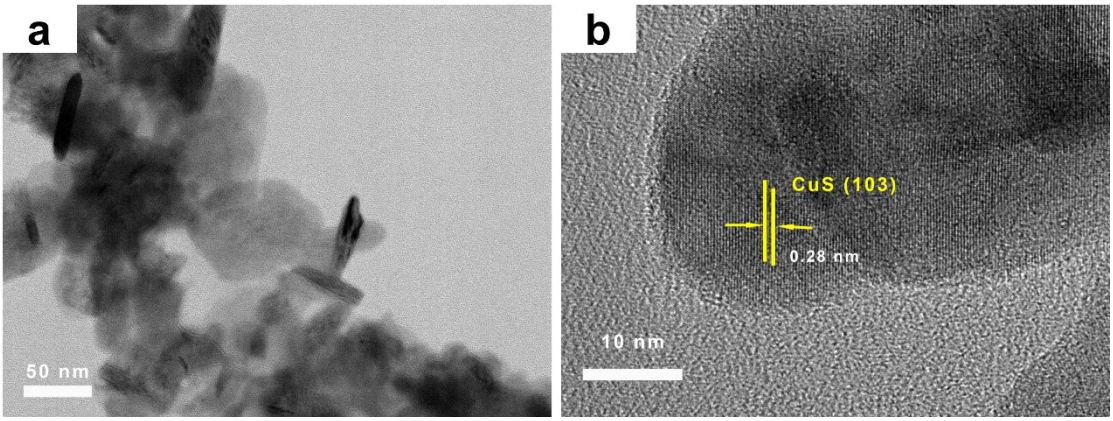

Figure S3. TEM (a) and HRTEM (b) images of CuS.

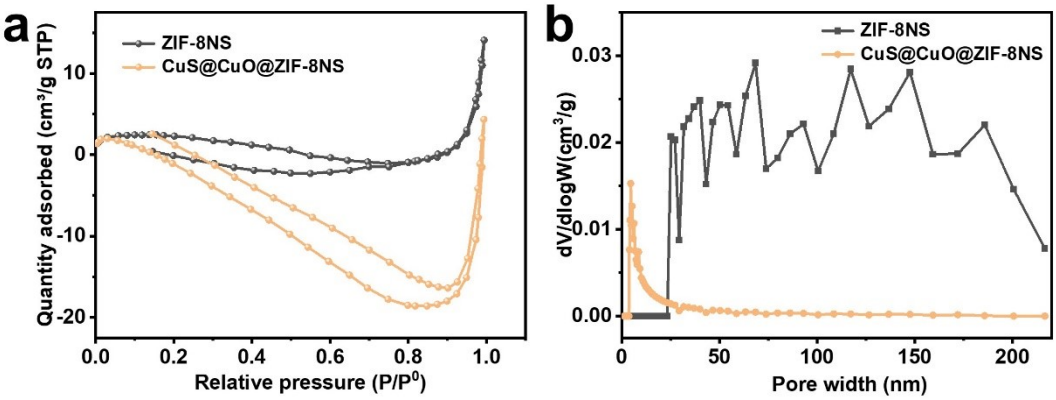

Figure S4. N_2-BET curves (a) and corresponding pore width (b) of catalysts.

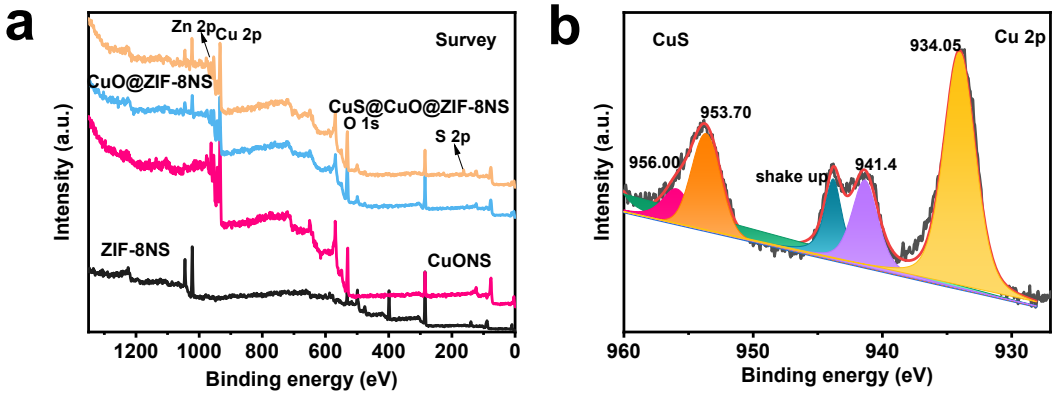

Figure S5. XPS Survey (a) and Cu 2p (b) of samples.

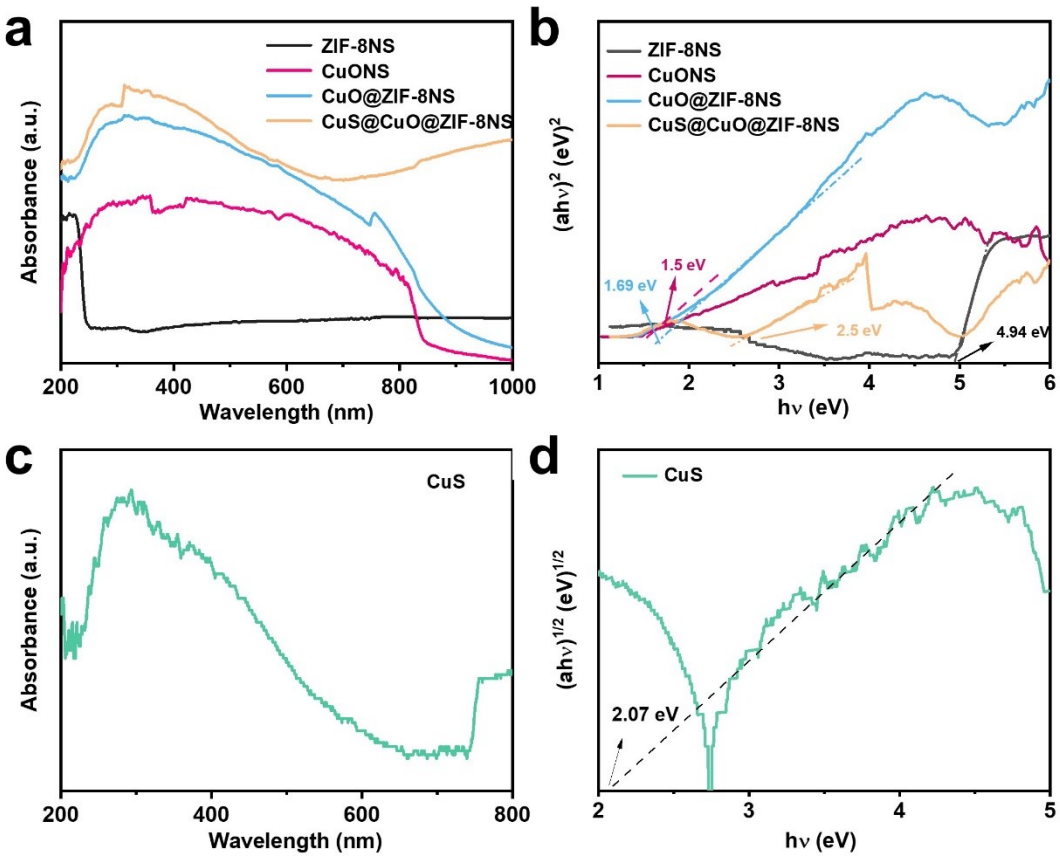

Figure S6. UV-vis absorption spectra (a), (c) and corresponding Tauc's band gap plots (b), (d) of catalysts

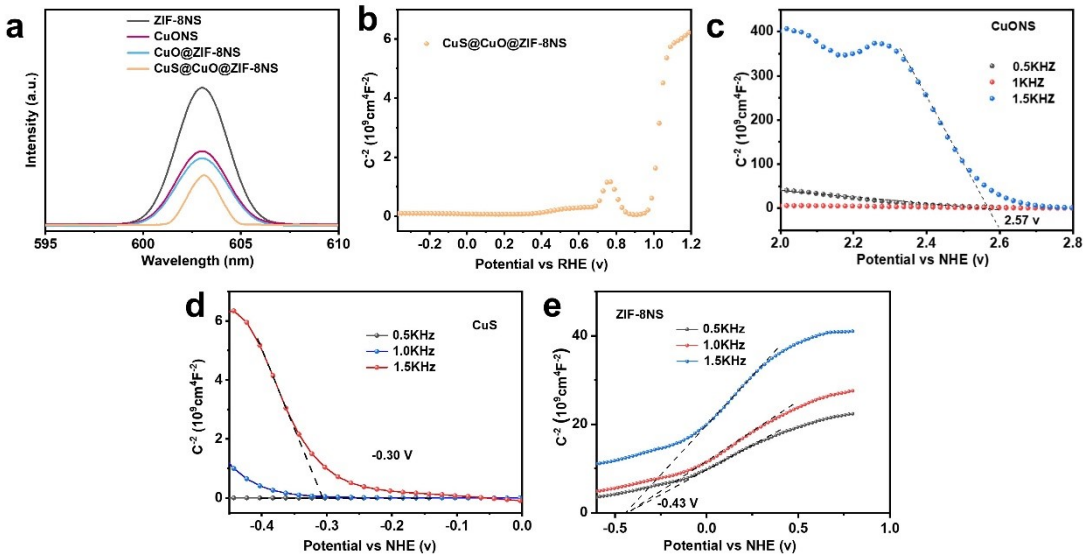

Figure S7. PL spectra(a), Mott-Schottky curves (b-e) of different samples.

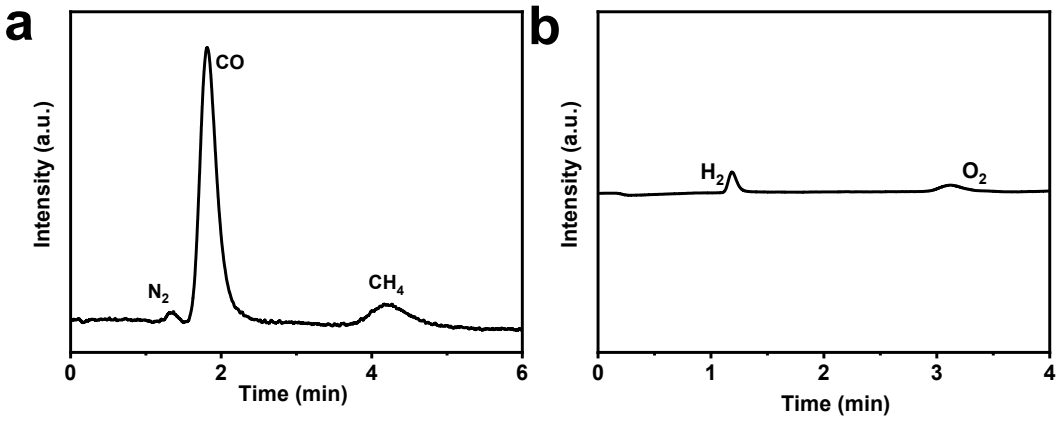

Figure S8. Gas chromatogram for FID (a) and TCD (b) over CuS@CuO@ZIF-8NS under solar irradiation.

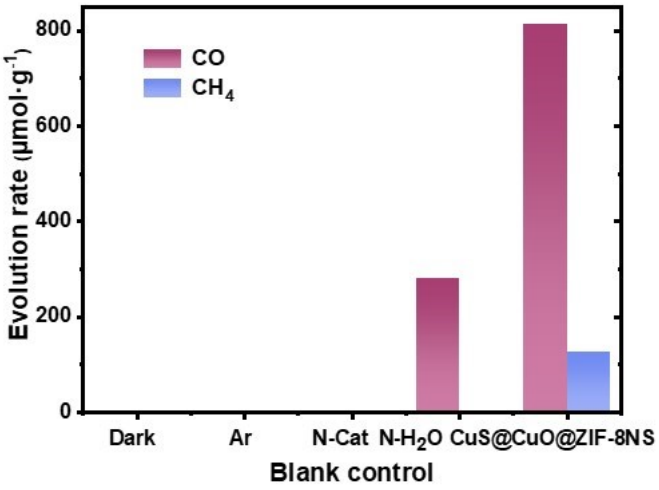

Figure S9. Average evolution yields of CO and CH_4 under different conditions.

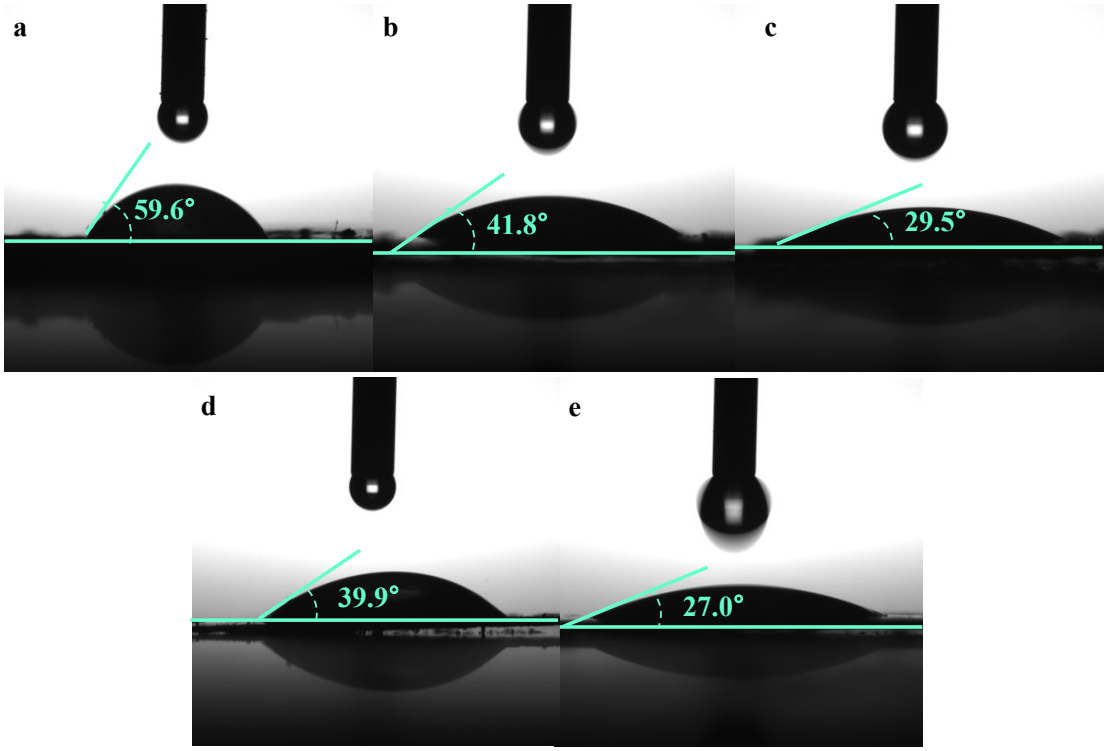

Figure S10. Contact Angle Test of ZIF-8NS(a), CuONS (b), CuO@ZIF-8NS, (c) CuS (d) and CuS@CuO@ZIF-8NS (e).

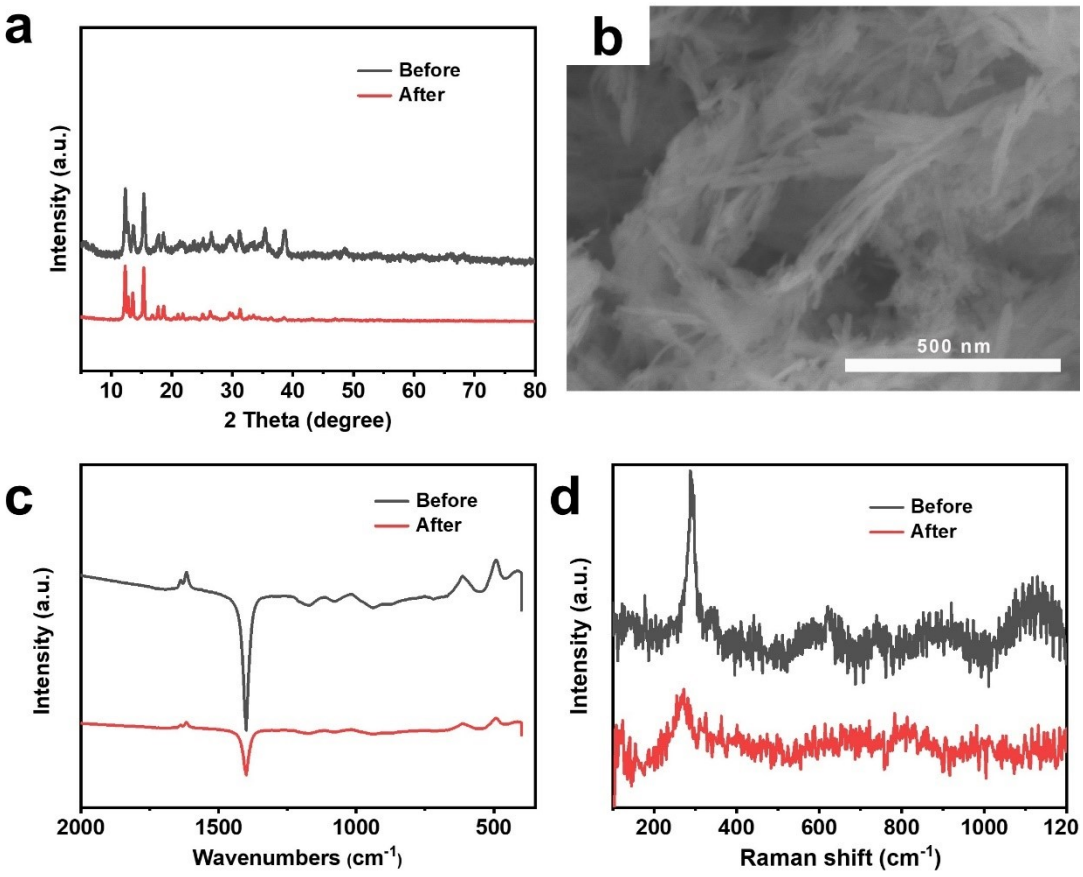

Figure S11. (a) XRD pattern (d) SEM, FTIR (c) and Raman (d) images of CuS@CuO@ZIF-8NS before and after four cycles reaction.

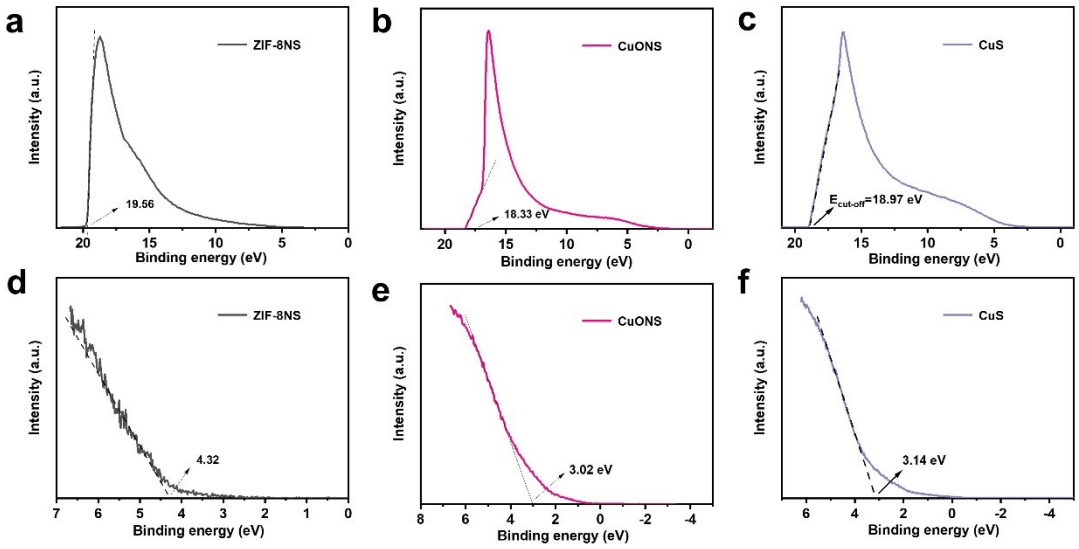

Figure S12. Ultraviolet photoelectron spectroscopy (UPS) test of samples.

2. Tables

Table S1 Summary of the specific surface aera (S_{BET}), pore volume and average pore size of the prepared samples.

Catalyst	S_{BET} (m^2 g^{-1}) [a]	Pore volume (cm^3 g^{-1}) [b]
ZIF-8NS	10.2842	0.005
CuS@CuO@ZIF-8NS	36.9263	0.016

[a] Surface area obtained by t-Plot method;

[b] Pore width determined by Horvath-Kawazoe method;

Table S2 The determined energy band parameters of the samples.

Sample	E_g (eV)	E_f	E_{VB} (eV)	E_{CB} (eV)
ZIF-8NS	4.94	-0.43	1.48	-3.46
CuONS	1.50	-0.30	1.41	-0.09
CuS	2.07	2.57	0.89	-1.18

Table S3 The photoluminescence decay time (τ) and their relative intensities of charge carriers in the samples.

Sample	τ_1 (ns)	τ_2 (ns)	A_1	A_2	Average-lifetime (τ,ns)
ZIF-8NS	0.56	1.39	-51.48	0.33	0.39
CuONS	0.12	0.82	4.33	0.39	0.16
CuS	0.37	0.87	-35.88	0.37	0.86
CuO@ZIF-8NS	0.18	0.97	0.21	0.35	0.90
CuS@CuO@ZNS	1.21	1.21	-0.33	0.33	1.21

The average lifetime was calculated using equation: $(\tau) = (I_1\tau_1^2+I_2\tau_2^2)/(I_1\tau_1+I_2\tau_2)$

Table S4 Comparative values of charge transfer resistance and solution resistance of the samples.

Sample	R_s (Ω)	R_{ct} (Ω)	C_d (μF)
ZIF-8NS	82.84	604.2	0.84
CuONS	80.75	425.3	0.83
CuO@ZIF-8NS	83.28	166.9	0.76
CuS@CuO@ZIF-8NS	80.43	105.2	0.75

Table S5 O_2 formation of CO_2 photoreduction over different samples under solar irradiation in TCD detector.

Sample	O_2 formation rate (μmol g^{-1} h^{-1})	
	Measured	Theoretical
ZIF-8NS	10.35	11.95
CuO@ZIF-8NS	34.45	40.57
CuS	24.12	26.34
CuO@ZIF-8NS	62.23	64.18
CuS@CuO@ZIF-8NS	155.96	157.41

The air residuals (N_2+O_2) were tested before light irradiation in each experiment. The O_2 generation was obtained by subtracting the air residuals. The theoretical rate of O_2 formation was calculated by (O_2 formation rate) = [(CO formation rate)/2+(CH_4 formation rate) ×2].

Table S6 Apparent quantum efficiencies (QE%) and solar-to-chemical fuel conversion efficiencies (CE%) of as-prepared samples.

Samples	Yield rate of CO ($\mu mol\ g^{-1}\ h^{-1}$)	Yield rate of CH_4 ($\mu mol\ g^{-1}\ h^{-1}$)	Selectivity (%)	CE (%)	QE (%)
ZIF-8NS	18.93	1.24	CO 93.85 CH_4 6.15	0.0034	3.91
CuONS	49.65	7.87	CO 86.32 $CH_4$13.68	0.011	13.30
CuS	34.80	4.47	CO 88.61 CH_4 11.39	0.0072	8.62
CuO@ZIF-8NS	85.80	10.64	CO 88.97 CH_4 11.03	0.0176	21.00
CuS@CuO@ZIF-8NS	270.96	44.57	CO 85.87 CH_4 14.2	0.0422	51.50

Table S7 Comparison of the activity of CuS@CuO@ZIF-8NS in the photocatalytic CO_2 reduction with the catalysts recently reported.

Photocatalyst	Solvent	Light resource	Major products (μmol g^{-1} h^{-1})	Selectivity (%) [a]	References
TiO_2/C@ZnCo-ZIF-L	H_2O	300 W Xe lamp	CO 28.6	--	Ref. 51[51]
TiO_2@UiO-66	H_2O	150 W and 300 W, λ > 325 nm.	CO 1.8	--	Ref. 52[52]
Au@ZIF-67	--	100 W, LCS-100 Xe lamp (λ < 400 nm)	CO 0.97 g/cm^3	--	Ref. 53[53]
UiO-66-NH_2-LV	H_2O, TEOA	300 W xenon lamp (400 nm ≤ λ)	CO 30.5	--	Ref. 54[54]
MIL-125-NH_2(Ti)	CH_3CN H_2O, TEOA	300 W xenon arc lamp with AM 1.5 G filter	CO 15.49 CH_4 5.46	93.1	Ref. 55[55]
ZIF-8	TEOA, H_2O, MeCN	300 W xenon lamp (>400nm)	CO 4.2	--	Ref. 56[56]
H-CdS@ZIF-8/Au	H_2O	300 W Xenon lamp (420 < λ < 780 nm)	CO 233.8	CO 90.7	Ref. 57[57]
BIF-20@g-C_3N_4	MeCN, TEOA	300 W xenon (420 ≤ λ ≤ 800 nm)	CO 53.869 CH_4 15.524	--	Ref.58[58]
ZIF-8/COF	H_2O	LED lamp	CO 84.87	CO 91	Ref. 59[59]
CuS@CuO@ZIF-8NS	**H_2O (gas)**	**300 W Xenon lamp**	**CO 270.96 CH_4 44.57**	**CO 85.8 CH_4 14.1**	**This work**

References

51. A.W. Zhou, Y.B. Dou, C. Zhao, J. Zhou, X.Q. Wu, J.R. Li, *Appl. Catal. B*, 2019, **264**, 118519.

52. A. Crake, K.C. Christoforidis, A. Gregg, B. Moss, A. Kafizas, C. Petit, *Small*, 2019, **15**, 1805473.

53. T. Tian, J. Xu, A. Abdolazizi, C. Ji, J. Hou, D.J. Riley, C. Yan, M.P. Ryan, F. Xie, C. Petit, *Mater. Today Nano*, 2023, **21**, 100293.

54. S.Q. Wang, X. Gu, X.Z. Wang, X.Y. Zhang, X.Y. Dao, X.M. Cheng, J. Ma, W.Y. Sun, Defect-engineering of Zr(IV)-based metal-organic frameworks for regulating CO_2 photoreduction, *Chem. Eng. J.*, 2022, **429**, 132157.

55. X.M. Cheng, Y.M. Gu, X.Y. Zhang, X.Y. Dao, S.Q. Wang, J. Ma, J. Zhao, W.Y. Sun, *Appl. Catal. B*, 2021, **298**, 120524.

56. Z.G. Liu, Z.Y. Chen, M.Y. Li, J.Y. Li, W.J. Zhuang, X. Yang, S.Q. Wu, J.L. Zhang, *ACS Catal.*, 2023, **13**, 6630-6640.

57. W.H. Mo, Z.X. Fan, S.X. Zhong, We.B. Chen, L.X. Hu, H. Zhou, W. Zhao, H.J. Lin, J. Ge, J.R. Chen, S. Bai, *Small*, 2023, **19**, 2207705.

58. G.L. Xu, H.B. Zhang, J. Wei, H.X. Zhang, X. Wu, Y. Li, C.S. Li, J. Zhang, J.H. Ye, *ACS Nano*, 2018, **12**, 5333-5340.

59. R.G. Yang, Y.M. Fu, H.N. Wang, D.P. Zhang, Z. Zhou, Y.Z. Cheng, X. Meng, Y.O. He, Z.M. Su, *Chem. Eng. J.*, 2022, **450**, 138040.